Chinese Journal of Aeronautics, (2025), 38(7): 103474

Chinese Society of Aeronautics and Astronautics
& Beihang University

Chinese Journal of Aeronautics

cja@buaa.edu.cn
www.sciencedirect.com

FULL LENGTH ARTICLE

Density measurements of aviation kerosene RP-3 over temperature range from 323 K to 783 K under supercritical pressures from 6 MPa to 8 MPa

Yanchen FU [a,b], Weitong LIU [a,b], Shenzhou SHI [c], Ruoyu WANG [a,b], Yinlong LIU [a,b], Guoqiang XU [a,b,*]

[a] *Research Institute of Aero-engine, Beihang University, Beijing 100191, China*
[b] *Collaborative Innovation Center for Advanced Aero-Engine, Beihang University, Beijing 100191, China*
[c] *Beijing Power Machinery Institute, Beijing 100074, China*

Received 18 June 2024; revised 22 July 2024; accepted 8 September 2024
Available online 10 March 2025

KEYWORDS

Aviation kerosene;
Density measurement;
High temperature;
Supercritical pressure;
Thermal properties

Abstract Aviation kerosene RP-3 is extensively used in China. This paper details the measurement of the density of Chinese aviation kerosene RP-3 employing the flow method under high-pressure and high-temperature conditions. The methodology utilizes circular tubes with two different diameters. The density of aviation kerosene RP-3 was experimentally measured for the first time within a pressure range from 6 MPa to 8 MPa and a temperature range from 323 K to 783 K, with a maximum relative uncertainty of 0.35%. The experimental setup used n-decane for calibration, achieving an average calibration error of 0.91%. The data indicate that the density of RP-3 ranges from 764 kg/m^3 to 247 kg/m^3 under the tested conditions. The results show that the density of kerosene RP-3 decreases with an increase in temperature at a constant pressure, and at a given temperature, a higher pressure results in a higher density. Polynomial fitting was applied to the data, resulting in the average absolute deviation of 1.09%, 0.80%, and 0.76% at different pressures of 6, 7, and 8 MPa, respectively.

1. Introduction

The pressing need to increase the speed of aircraft has led to progressively higher temperatures in the thermal components of aero engines, resulting in more severe thermal loads and a greater demand for cooling technologies.[1–3] However, the efficiency of the commonly used air-cooling technologies decreases due to the rising compression ratio of the compres-

* Corresponding author.
E-mail address: guoqiang_xu@buaa.edu.cn (G. XU).
Peer review under responsibility of Editorial Committee of CJA

Production and hosting by Elsevier

https://doi.org/10.1016/j.cja.2025.103474

sor. Consequently, the Cooled Cooling Air technology (CCA)[4–6] with air–fuel heat exchangers, utilizing the heat sink of the airborne endothermic hydrocarbon fuel to enhance the cooling capacity of the air, has emerged.[7–9] Major aviation fuels, such as JP-8 in the United States and RP-3 in China,[10] typically are mixtures of hundreds of various hydrocarbons. Moreover, currently, the pressure in aero-engine fuel systems is about 3.86–5.00 MPa, which exceeds the critical pressure of aviation fuels. The thermal properties of aviation kerosene undergo dramatic changes in the near-critical region, significantly impacting the flow and heat transfer characteristics of the fuel. These changes can lead to unique flow and heat transfer phenomena.[11–13] To effectively utilize the heat sink of the hydrocarbon fuel and optimize the air–fuel heat exchanger design, it is crucial to maintain a highly accurate database of fuel thermal properties at supercritical pressures. This database should primarily include density, viscosity, isobaric specific heat capacity, thermal conductivity, critical point, and saturated vapor pressure. Therefore, it is particularly important to accurately measure these thermal properties through experimental methods.

Density measurement methods are generally categorized into direct and indirect methods. Direct measurements, based on the definition of density (the mass of a substance per unit volume), include Archimedes method,[14] hydrostatic weighing,[15] pycnometry,[16,17] and hydrometer methods.[18,19] Indirect measurements, on the other hand, encompass techniques such as vibrational, radiographic, acoustic, pulsed excitation,[20] and thermal pulse methods.[21–28] The aforementioned direct and indirect methods are typically suitable only for measuring density under low-temperature and low-pressure conditions, and many unresolved issues remain for their application at high temperatures and pressures.

Specifically, methods like the Archimedes method, pycnometry, and hydrometry could only be used for offline measurement and are incapable of reflecting real-time changes in the density of the fluid under tests. Besides, these methods are not applicable under high-pressure conditions.[29–31] The vibrational measurement method is capable of measuring fluid density under high-pressure conditions; however, it is not suitable for high-temperature conditions[32,33]. Radiographic methods, typically involving the measurement of radiation attenuation, are frequently used for measuring fluid density under high temperature and pressure conditions.[34] However, these methods necessitate a minimum density of the test substance, and the radiation employed may pose risks to human health. The acoustic method, noted for its high sensitivity and automation, is a non-contact technique. However, it exhibits a significant error margin when measuring the density of two-phase fluids, and the uniformity of the fluid density being tested substantially influences the accuracy of the results.[35,36] Since the acoustic method has reached its limits, an improved method of using the oscillating U-tube principle, the pulsed excitation method, has been developed in 2019.[37] This method could gain three times more information than the conventional acoustic method. However, it is not suitable for high-temperature conditions, with a maximum temperature of 150 °C.[38]

Gülüm and Bilgin[39] measured the density of biodiesel-diesel blends at the temperatures of 10, 20, 30, and 40 °C by means of the pycnometer. Bruno et al.[24] conducted density measurements on the hydrocarbon fuel JP-10 over the temperature range from 233.15 K to 373.15 K at the pressure of 84 kPa, with a maximum measuring error of −0.22%. Wen et al.[40] measured the density of propellant EHF-TU over a temperature range of 303–765 K and a pressure range of 3–7 MPa with an uncertainty of 1.1%. The density of an endothermic hydrocarbon fuel was measured online by Yang et al.[41] employing a radial measurement method, covering the temperature range of 283–950 K at the pressure of 3 MPa and 4 MPa. And the uncertainty of their measurements was 0.292% to 2.286%. Deng et al.[42] measured the density of hydrocarbon fuel RP-3 at sub- and supercritical conditions over a temperature range of 295–796 K and a pressure range of 2–5 MPa. The results indicate that the density of RP-3 at the critical point is 221.18 kg/m^3. Although some studies have been conducted on the density measurement of endothermic hydrocarbon fuels under high temperatures and pressures, the uncertainty of existing methods remains high. Additionally, there is a lack of density data for Chinese aviation kerosene RP-3 at high temperatures (300–800 K) and high pressures (6–8 MPa).

The current study introduces a novel method for measuring fluid density under high temperatures and pressures. For the first time, the density of aviation kerosene RP-3 has been measured using a flow method with low uncertainty in the temperature range of 323–783 K and pressure range of 6–8 MPa.

2. Experimental setup

2.1. Aviation kerosene RP-3 properties

Chinese aviation kerosene RP-3 plays a crucial role in the field of aerospace engineering due to its distinctive properties and applications. This hydrocarbon fuel is a complex mixture derived from the fractional distillation of crude oil, characterized by its high-energy content and stability under varying operational conditions. RP-3 is specifically formulated to meet the rigorous demands of aviation, offering a balance between high calorific value and low-temperature performance, which is essential for efficient aircraft operation. Its formulation is tailored to ensure optimal combustion efficiency, reduced carbon emissions, and minimal impact on engine operating life. RP-3 kerosene is composed of 92.1% saturated hydrocarbons and 7.9% aromatic hydrocarbons by volume. The specific

Table 1 Components of aviation kerosene RP-3.[43]

Composition		Volume fraction (%)
Saturated hydrocarbons	Alkanes	52.2
	Monocyclic naphthenes	33.8
	Bicyclic naphthenes	6.0
	Tricyclic naphthenes	0.1
Aromatic hydrocarbons	Alkyl benzenes	5.1
	Indan tetralin	1.3
	Naphthalene	0.6
	Naphthalene derivatives	0.9

components of RP-3, detailed in Table 1,[43] include saturated straight-chain alkanes, naphthenes, and aromatic compounds.

The critical point of aviation kerosene RP-3 is T_c = 645.04 K, P_c = 2.33 MPa.[44] The flash point of RP-3 is 50 °C, its molar mass is 148.33 g/mol, and its boiling point ranges from 163 °C to 212 °C.[45] The average molecular formula of RP-3 is $C_{10.5}H_{22}$. Under standard conditions (1 atm (1 atm = 101 325 Pa), 20 °C), its density is 791.3 kg/m^3.

The importance of RP-3 transcends its basic function as a fuel. Due to its thermal properties, especially under high-temperature and high-pressure conditions, currently, the thermal–hydraulic performance of RP-3 is a critical research subject for thermal management in aero engines.[46,47] As aero engines operate at higher temperatures to achieve greater efficiencies and speeds, RP-3 also becomes a coolant. Therefore, it is necessary to thoroughly understand the physical and chemical properties of RP-3 under various operating conditions.

2.2. Experimental system

An experimental system for investigating supercritical hydrocarbon fuel flow and heat transfer characteristics has been established, as shown in Fig. 1. The experimental setup comprises four main sub-systems: supply section, heating section, measurement section, and recovery section. In the supply system, kerosene RP-3 is pumped from the storage tank using high-pressure-resistant liquid pumps (SP6015: 15 MPa, 0.01–600.00 mL/min; LP-0110: 15 MPa, 0.01–999.99 mL/min). The mass flow rate of the RP-3 could also be adjusted by the pump and measured using a Coriolis mass flowmeter (DMF-1–1). Subsequently, the RP-3 flows into a two-stage preheating section consisting of two electrically heated serpentine tubes, where it is heated to the target temperature. The density measurements of RP-3 under different temperatures and pressures will be conducted in the measurement section, and the details will be introduced in Section 2.3. After completing density measurements, high-temperature RP-3 flows into a water cooler and then flows through a back pressure valve that controls the system pressure. Finally, the used kerosene RP-3 flows into another tank for collection and storage. During the experiments, electrical signals, including pressure and mass flow rate, are collected using the data acquisition modules Adam-4118 and Adam-4520.

2.3. Test section

The test section is illustrated in Fig. 2. The main body of the test section consists of two vertically placed thin cylindrical tubes and a horizontally placed circular tube. Thermocouples (KPS-WRNK-191, range: −50 °C to 1 300 °C) are installed at both the inlet and outlet of the horizontal tubes to measure the entering and exiting temperature of the RP-3. The outer surface of the horizontal tube is wrapped with resistance wire for electrical heating, and the entire test section is encased in insulation material ASPEN with a thermal conductivity of 0.012 W/(m·K) to minimize heat loss. When the inlet and outlet temperatures are equalized, it is assumed that heat loss is negligible, and measurement experiments could begin. At the inlet of the horizontal tube, two copper electrodes connected to a programmable power supply are positioned to apply different waveforms of electrical pulses. This process induces temperature fluctuations by electrically heating the tube wall. The collection and recording of temperature fluctuation data are

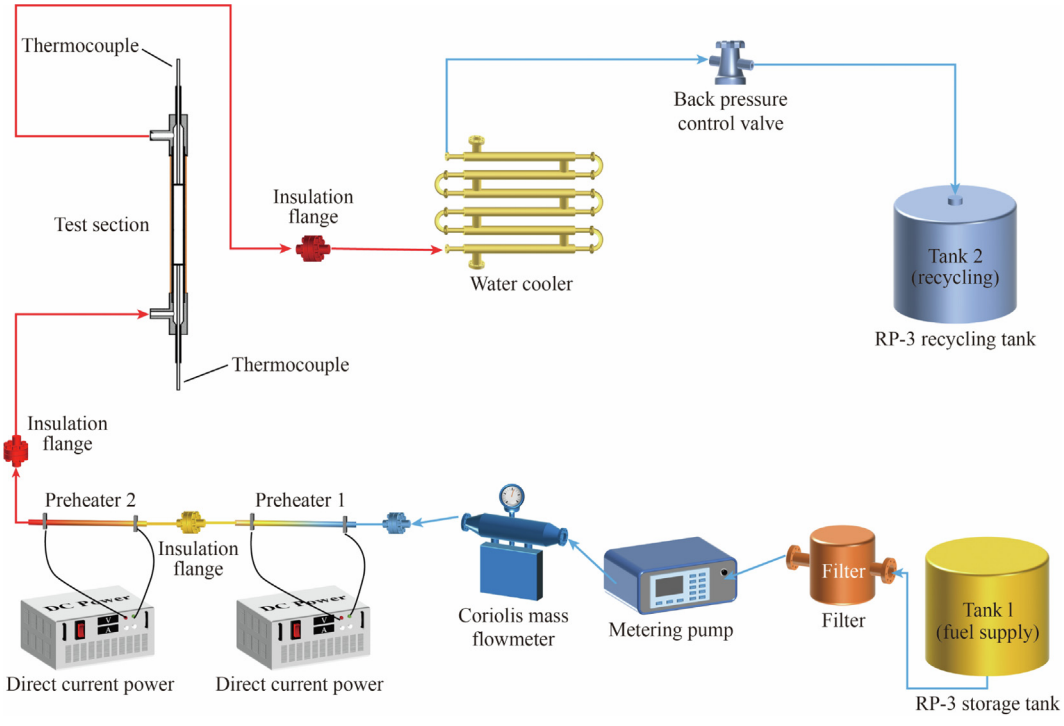

Fig. 1 Schematic of supercritical hydrocarbon fuel flow and heat transfer experimental system.

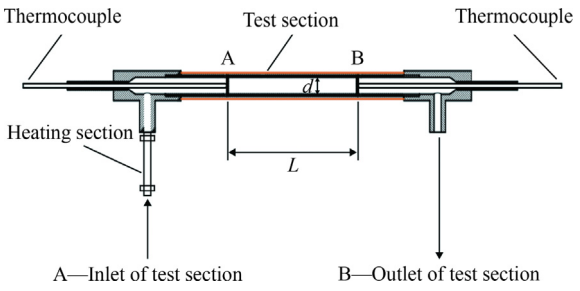

Fig. 2 Schematic of test section.

accomplished using a Yokogawa high-speed acquisition module (module VZ20X) and GA10 data logging software. The module VZ20X is an analog signal acquisition unit capable of high-speed, high-precision, and synchronized measurement of various analog signals. It features eight analog input channels per unit and supports high-speed sampling (1 kHz). The input channels are insulated from each other, ensuring reliable measurements in noisy environments.

3. Theory and uncertainty analysis

3.1. Theory

The flow method measures the density of flowing hydrocarbon fuel based on the principle of mass conservation. Details of the experimental application and theoretical basis can be found in our past work.[40,42] In a leak-free tube, the fluid mass flow rate remains the same from the inlet to the outlet and can be calculated by the formula below:

$$m = \rho U A \tag{1}$$

where A is the cross-sectional area of the tube, ρ and U represent the fluid density and average velocity, respectively.

Measurement of mass flow rate m could be taken by precise flowmeter. The cross-sectional area of the tube depends on the tube diameter (d) and could be calculated by the following equation:

$$A = \frac{\pi d^2}{4} \tag{2}$$

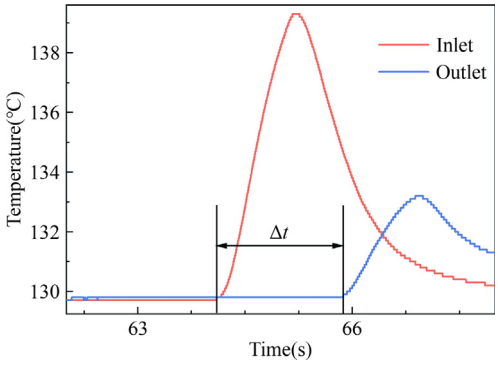

Fig. 3 Response of thermocouples and residence time collected and filtered by VZ20X.

Combining Eq. (1) and Eq. (2), the density of the flowing fluid could be calculated with the average velocity, which is the key to the flow method for density measurement. The proposed flow method is actually an approach to measure the average velocity with high accuracy. As depicted in Fig. 2, within a straight tube, thermocouples are positioned separately at the inlet and outlet. The inlet thermocouple detects changes in fluid temperature earlier than the outlet thermocouple when the fluid is heated prior to entering the tube. The response of thermocouples is represented in Fig. 3.

The time difference between the thermocouples at the inlet and outlet theoretically equals the residence time of the fluid flowing through the center of the tube. Therefore, the fluid average velocity between the thermocouples at the inlet and outlet can be calculated as follows:

$$U = \frac{L}{\Delta t} \tag{3}$$

where L is the length between the inlet and outlet thermocouples, and Δt is the residence time. By combining Eqs. (1)–(3), the density of the fluid flowing inside a straight circular tube could be measured using the formula below:

$$\rho = \frac{4m\Delta t}{\pi d^2 L} \tag{4}$$

Integrating Eq. (4) with the prior analysis indicates that the accuracy of this density measurement method is directly and significantly influenced by the measurements of mass flow rate, tube diameter, tube length, and residence time. The first three parameters have matured into highly reliable and precise instruments and measurement methods. In other words, the measurement of residence time contributes more significantly to the measuring errors. The measurement of residence time is a transient process comprising three parts: the increase in fluid temperature, the response of the thermocouple along with the change in temperature difference, and the acquisition of the voltage signal by the acquisition module. These three parts represent the major direction for optimization in this study. Compared to Deng's study,[42] the current study adopts thermocouples with faster responses. Moreover, the acquisition frequency has been increased to five times the original, with the acquisition delay reduced to 0.001 s. In addition, a power supply frequency noise removal filter has been added to the original data processing to optimize the identification and acquisition of residence time.

3.2. Uncertainty analysis

Based on Eq. (4), the density measurement demands mass flow rate, tube diameter, length of test section, and residence time. The uncertainty of the former three parameters largely relies

Table 2 Uncertainty of direct measurements.

Parameter	Measuring device	Uncertainty
Mass flow rate	Coriolis mass flowmeter	0.15%
Tube diameter	Scanning electron microscope	0.001 mm
Length of test section	Vernier caliper	1 mm

on the accuracy of the instrument. The uncertainty of the instruments used in the present study is listed in Table 2.

Since the residence time is measured by thermocouples through the high-speed acquisition module, the time response of the thermocouples and the frequency of the acquisition module contribute to the dominant uncertainty. The thermocouple time response constant τ_c is calculated by the following equation[48]:

$$\tau_c = \frac{\rho_{tc} c_{p,tc} V_{tc}}{h A_{tc}} \tag{5}$$

where ρ_{tc} and $c_{p,tc}$ are respectively the density and isobaric specific heat capacity of the thermocouple; V_{tc} and A_{tc} are the volume and surface area of the thermocouple's tip, respectively; and h represents the heat transfer coefficient. The thermocouple theoretical response relation[48] is

$$\frac{T - T_0}{T_\infty - T_0} = 1 - \exp\left(-\frac{\tau - \tau_s}{\tau_c}\right) \tag{6}$$

where T is the fluid transient temperature measured by the thermocouple; T_0 and T_∞ are the initial temperature and the final temperature, respectively; τ is the measurement time by the acquisition module and τ_s represents the start time point of thermocouple response to the thermal pulse.

In the experiment, the minimum sensitivity ($T - T_0$) of the used thermocouples is 0.15 K, and the final temperature difference ($T_\infty - T_0$) caused by typical thermal pulses is generally not less than 10 K. Furthermore, the thermocouple time constant response, τ_c, for RP-3 varies with temperature: approximately 0.15 s when the fluid temperature is below 643 K, 0.3 s in the pseudo-critical temperature region (643–683 K), and 0.03 s when the temperature exceeds 683 K. Based on the aforementioned data, the response time of the thermocouples is calculated to be: 2.27 ms when the fluid temperature is below T_c, 4.53 ms in the pseudo-critical temperature region, and 0.45 ms when the temperature exceeds T_c. The sampling interval time of the high-speed acquisition module is 1 ms, with a sampling uncertainty of 0.1 ms. Since the response time of the thermocouples at different temperatures all exceed the uncertainty of the high-speed acquisition module, it could be considered that the uncertainty in residence time is primarily due to the response time of the thermocouples. During the experiment, the residence time is controlled at over 1.5 s between 643 K and 683 K, and over 1 s below 623 K and above 683 K.

Based on the analysis above, the uncertainties of residence time Δt within different temperature ranges are as follows: 0.227% when the fluid temperature is below 623 K, 0.302% when the fluid temperature is within the pseudo-critical temperature region (643–683 K), and 0.045% when the fluid temperature is above 683 K.

The relative uncertainty of the fluid density measurement is calculated according to the following equation:

$$\varepsilon(\rho) = \sqrt{\varepsilon^2(m) + \varepsilon^2(L) + 4\varepsilon^2(d) + \varepsilon^2(\Delta t)} \tag{7}$$

The final calculation yields the relative uncertainty for the fluid density measurement within different temperature ranges: 0.29% when the fluid temperature is below 623 K, 0.35% when the fluid temperature is within the pseudo-critical temperature region (643–683 K), and 0.19% when the fluid temperature is above 683 K.

4. Results and discussion

4.1. Calibration using n-decane

To verify the reliability of the proposed density measurement method and the experimental system, it is necessary to conduct calibration experiments before formal measurements. n-decane is selected as the calibration fluid, with the system pressure maintained at 3 MPa and 6 MPa and temperature ranges of 304–698 K. n-decane is a colorless liquid with a critical temperature of 617.7 K and a critical pressure of 2.103 MPa. The mass flow rate, tube diameter, and tube length are selected as needed based on different temperature ranges to ensure the flow Reynolds number greater than 5 000 and sufficient residence time. The experimentally measured density (ρ_{exp}), standard n-decane density (ρ_{real}) from the NIST (National Institute of Standards and Technology) REFPROP database,[49] and their relative deviations are listed in Tables 3 and 4. The Relative Deviation (RD), Average Absolute Deviation (AAD), and Maximum Absolute Deviation (MAD) are calculated as follows.

$$\mathrm{RD} = \frac{\rho_{exp} - \rho_{real}}{\rho_{real}} \tag{8}$$

$$\mathrm{AAD} = \frac{1}{n}\sum_{i=1}^{n}\left|\frac{\rho_{exp,i} - \rho_{real,i}}{\rho_{real,i}}\right| \tag{9}$$

$$\mathrm{MAD} = \max\left\{\left|\frac{\rho_{exp,i} - \rho_{real,i}}{\rho_{real,i}}\right|\right\} \tag{10}$$

Fig. 4 demonstrates the RD of n-decane variations with n-decane temperature. The AAD of the n-decane in the experiments is 0.91% and the MAD is 3.04%. The measurement deviation for density between 600 K and 700 K is generally larger than that between 300 K and 600 K. This is because, in the pseudo-critical region, the density undergoes significant fluctuations.

In fact, prior to the aforementioned calibration experiments, we also conducted a pre-calibration using n-decane to optimize our measurement methods. Fig. 5 shows the results of our pre-calibration. In the pre-calibration experiments using n-decane, the pressure was maintained at 3 MPa, with a tem-

Table 3 Experimentally measured density ρ_{exp}, standard n-decane density ρ_{real}, and relative deviation of n-decane at 3 MPa over temperature ranges of 304–604 K.

T (K)	ρ_{exp} (kg/m^3)	ρ_{real} (kg/m^3)	RD (%)
304.04	734.56	724.35	1.41
324.03	710.72	709.10	0.23
373.41	668.82	670.98	−0.32
393.03	644.06	655.45	−1.74
403.85	633.35	646.75	−2.07
423.33	630.86	630.78	0.01
423.65	623.88	630.51	−1.05
463.48	601.80	596.13	0.95
503.38	565.62	558.21	1.33
543.68	520.70	513.79	1.35
573.44	474.90	473.79	0.23
603.56	419.60	420.42	−0.19

Table 4 Experimentally measured density ρ_{exp}, standard n-decane density ρ_{real}, and relative deviation of n-decane at 6 MPa over temperature ranges of 598–698 K.

T (K)	ρ_{exp} (kg/m^3)	ρ_{real} (kg/m^3)	RD (%)
598.40	477.21	468.25	1.91
623.30	445.46	435.74	2.23
648.08	407.14	400.01	1.78
673.14	365.32	360.49	1.34
698.29	319.90	317.72	0.69

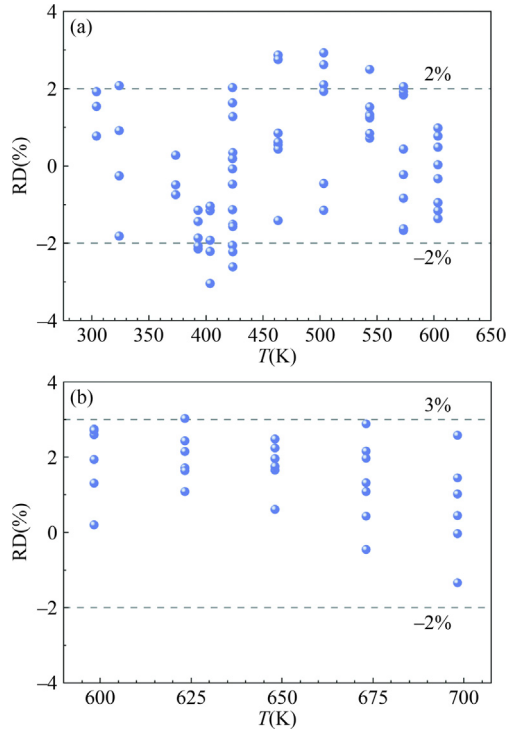

Fig. 4 RD of n-decane variations with n-decane temperature: (a) n-decane at P = 3 MPa and temperature ranges from 304 K to 603 K; (b) n-decane at P = 6 MPa and temperature ranges from 598 K to 698 K.

perature range of 150 °C to 450 °C, and a mass flow rate of 3 g/s. It can be seen that the pre-calibration experiments exhibit significant errors in both the low-temperature region (below 200 °C) and the high-temperature region (above 400 °C). This is because, in the low-temperature region, the fluid viscosity is higher and the Reynolds number is lower, resulting in flow being laminar or in transition, with an uneven velocity distribution; in the high-temperature region, the density of n-decane decreases rapidly, leading to a shorter residence time in the test section, and thus significant errors in residence time measurement. On the basis of the experience gained from pre-calibration experiments, principles that contribute to the accuracy of measurements have been summarized: (A) Ensuring the fluid in the test section is in the turbulent regime. This is due to the presence of a boundary layer when fluid flows inside the

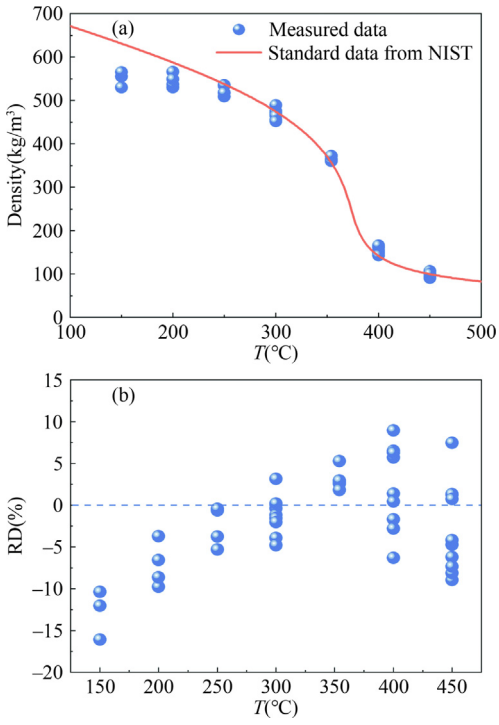

Fig. 5 Pre-calibration results with high error: (a) Comparison of n-decane density between measured data with standard data; (b) RD of n-decane variations with temperature.

tube, where the velocity gradient is significant, causing an uneven velocity field distribution across the cross-section of the tube. Compared to laminar flow, under the same flow conditions, the velocity field distribution of the fluid is more uniform in turbulent flow.[50,51] Therefore, the average fluid velocity measured through residence time in turbulent flow is closer to the actual mainstream velocity, which could significantly enhance the measurement accuracy. (B) The residence time should not be excessively long or short. In this experiment, temperature fluctuations are captured using a high-speed acquisition module to determine residence time. On one hand, excessively long residence times cause temperature fluctuations to become less pronounced due to axial heat conduction during tests, making them more difficult to be measured by thermocouples. On the other hand, the high-speed acquisition module has a sampling interval of 1 ms, and excessively short residence times increase the uncertainty of its measurements. Based on these experiential guidelines, two test sections with different diameters and lengths were designed to measure the density of RP-3 under different temperatures and pressures.

4.2. Density measurement of RP-3

The density of RP-3 has been measured at temperature ranges from 323 K to 783 K and pressure ranges from 6 MPa to 8 MPa. Fig. 6 shows the response curves of the thermocouples at the inlet and outlet of the experimental section under typical conditions over time. It can be observed that after the heat pulse is applied, the inlet thermocouple responds first, showing

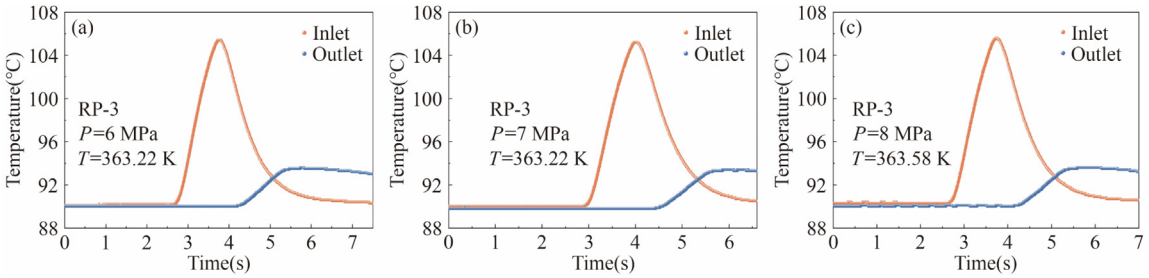

Fig. 6 Response of inlet and outlet thermocouples with time under typical conditions: (a) P = 6 MPa, T = 363.22 K; (b) P = 7 MPa, T = 363.22 K; (c) P = 8 MPa, T = 363.58 K.

Table 5 Values of temperature polynomial coefficient C_i at different pressures.

Pressure (MPa)	C_1	C_2	C_3	C_4	C_5	C_6
6	−742.885	15.590	−0.059 0	1.018×10^{-4}	-8.235×10^{-8}	2.382×10^{-11}
7	340.372	4.358	−0.013 7	1.330×10^{-5}	1.497×10^{-9}	-6.871×10^{-12}
8	2 450.547	−16.027	0.063 7	-1.308×10^{-4}	1.332×10^{-7}	-5.401×10^{-11}

Table 6 Experimentally measured density of RP-3 at pressures of 6, 7, and 8 MPa and temperature ranges from 323 K to 783 K.

P (MPa)	T (K)	ρ_{exp} (kg/m^3)	ρ_{fit} (kg/m^3)	P (MPa)	T (K)	ρ_{exp} (kg/m^3)	ρ_{fit} (kg/m^3)	P (MPa)	T (K)	ρ_{exp} (kg/m^3)	ρ_{fit} (kg/m^3)
6	323.23	760.23	758.81	7	323.07	760.64	760.48	8	323.95	765.69	768.16
6	343.23	750.72	748.61	7	343.18	752.28	749.74	8	343.98	754.12	752.49
6	363.22	738.79	736.25	7	363.22	739.95	737.67	8	363.58	743.91	738.16
6	373.18	723.66	729.51	7	373.35	728.30	731.14	8	372.82	736.20	731.61
6	393.05	708.66	715.30	7	393.13	709.02	717.78	8	393.28	708.63	717.34
6	408.14	697.30	704.07	7	408.24	703.77	707.14	8	408.11	700.28	707.05
6	423.27	695.13	692.62	7	423.24	698.25	696.31	8	423.43	694.66	696.39
6	438.21	682.72	681.24	7	438.10	690.14	685.40	8	438.29	685.77	685.95
6	453.19	678.60	669.86	7	453.14	679.87	674.24	8	453.29	680.69	675.29
6	468.23	666.70	658.51	7	467.99	665.81	663.15	8	468.23	667.88	664.52
6	483.48	653.14	647.07	7	483.23	653.41	651.73	8	483.21	657.08	653.60
6	498.33	633.69	636.00	7	498.29	636.90	640.41	8	498.09	641.01	642.62
6	513.10	622.21	624.99	7	513.31	630.55	629.08	8	513.41	628.79	631.18
6	528.30	612.66	613.59	7	528.33	618.85	617.69	8	528.21	621.50	620.03
6	543.36	603.91	602.13	7	543.41	608.57	606.14	8	543.30	614.25	608.55
6	558.28	582.58	590.48	7	557.98	589.80	594.82	8	558.31	593.80	597.02
6	573.46	577.62	578.16	7	573.16	581.37	582.76	8	573.21	583.53	585.43
6	588.08	558.88	565.71	7	588.53	568.75	570.18	8	588.51	573.57	573.34
6	603.38	543.72	551.87	7	603.30	548.31	557.59	8	603.19	554.05	561.48
6	618.56	528.70	537.09	7	618.45	535.86	544.02	8	618.30	542.65	548.92
6	633.35	524.63	521.50	7	633.53	530.59	529.68	8	633.16	537.02	536.06
6	648.15	515.10	504.50	7	648.01	523.02	514.93	8	648.31	528.71	522.27
6	663.21	497.68	485.54	7	663.11	507.10	498.31	8	662.98	513.16	508.04
6	678.41	469.73	464.45	7	678.24	489.84	480.14	8	678.09	496.23	492.19
6	693.10	445.65	441.98	7	693.05	459.38	460.61	8	693.09	475.35	474.93
6	708.41	420.20	416.10	7	708.14	440.69	438.63	8	708.19	458.79	455.63
6	722.99	382.21	388.92	7	723.10	410.14	414.44	8	722.94	425.38	434.48
6	743.21	330.27	346.66	7	742.95	365.03	378.05	8	742.93	393.53	401.23
6	763.30	297.79	298.94	7	763.40	336.47	334.55	8	763.44	370.12	360.24
6	783.53	252.11	244.56	7	783.50	288.94	284.80	8	783.56	309.32	311.47

Table 7 Fitting deviations of RP-3 densities between experimentally measured data and fitted data.

P (MPa)	T (K)	ξ (%)	P (MPa)	T (K)	ξ (%)	P (MPa)	T (K)	ξ (%)
6	323.23	0.19	7	323.07	0.02	8	323.95	0.32
6	343.23	0.28	7	343.18	0.34	8	343.98	0.22
6	363.22	0.34	7	363.22	0.31	8	363.58	0.77
6	373.18	0.81	7	373.35	0.39	8	372.82	0.62
6	393.05	0.94	7	393.13	1.24	8	393.28	1.23
6	408.14	0.97	7	408.24	0.48	8	408.11	0.97
6	423.27	0.36	7	423.24	0.28	8	423.43	0.25
6	438.21	0.22	7	438.10	0.69	8	438.29	0.03
6	453.19	1.29	7	453.14	0.83	8	453.29	0.79
6	468.23	1.23	7	467.99	0.40	8	468.23	0.50
6	483.48	0.93	7	483.23	0.26	8	483.21	0.53
6	498.33	0.36	7	498.29	0.55	8	498.09	0.25
6	513.10	0.45	7	513.31	0.23	8	513.41	0.38
6	528.30	0.15	7	528.33	0.19	8	528.21	0.24
6	543.36	0.29	7	543.41	0.40	8	543.30	0.93
6	558.28	1.36	7	557.98	0.85	8	558.31	0.54
6	573.46	0.09	7	573.16	0.24	8	573.21	0.33
6	588.08	1.22	7	588.53	0.25	8	588.51	0.04
6	603.38	1.50	7	603.30	1.69	8	603.19	1.34
6	618.56	1.59	7	618.45	1.52	8	618.30	1.15
6	633.35	0.60	7	633.53	0.17	8	633.16	0.18
6	648.15	2.06	7	648.01	1.55	8	648.31	1.22
6	663.21	2.44	7	663.11	1.73	8	662.98	1.00
6	678.41	1.12	7	678.24	1.98	8	678.09	0.82
6	693.10	0.82	7	693.05	0.27	8	693.09	0.09
6	708.41	0.98	7	708.14	0.47	8	708.19	0.69
6	722.99	1.75	7	723.10	1.05	8	722.94	2.14
6	743.21	4.97	7	742.95	3.56	8	742.93	1.96
6	763.30	0.38	7	763.40	0.57	8	763.44	2.67
6	783.53	3.00	7	783.50	1.43	8	783.56	0.69

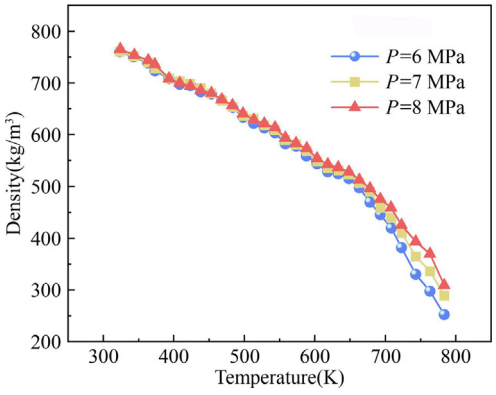

Fig. 7 Experimental density of RP-3 at pressures of 6, 7, and 8 MPa and temperature ranges from 323 K to 783 K.

a pulse-like change in temperature, followed by the outlet thermocouple receiving the heat pulse signal, with its temperature also changing accordingly. By following the theory mentioned in Section 3.1, the density of RP-3 under these conditions can be calculated. Besides, all experimentally measured RP-3 density data at constant pressure have also been fitted using a piecewise polynomial. The fitting formula is shown below.

$$\rho = \sum_{i=1}^{n} C_i T^{i-1} \tag{11}$$

where C_i represents the temperature polynomial coefficient, n is the number of the polynomial coefficients, determined through the F-test method.

Table 5 shows the values of C_i under different pressures. The fitting results are of high accuracy, with the coefficient of determination (R^2) of the fitting results being greater than 0.998 for the different pressures. Table 6 lists the experimentally measured RP-3 densities and the fitted RP-3 densities, while Table 7 provides the fitting deviations (ξ). The density variations of RP-3 with the temperature at the pressure of 6, 7, and 8 MPa are demonstrated in Fig. 7. Similar to pure substance fluids, the density of RP-3 decreases with an increase in temperature, a trend that is more pronounced near the pseudo-critical region. The critical pressure of RP-3 is 2.33 MPa.[44] Around a temperature of 650 K and under a pressure of 6 MPa, RP-3 enters the pseudo-critical region. Before reaching the pseudo-critical region, RP-3 exhibits liquid properties, with its density increasing as pressure rises, although it is not particularly sensitive to pressure changes. Once the temperature of RP-3 exceeds the pseudo-critical temperature and it enters the supercritical state, the density of RP-3 significantly decreases but still remains at a level close to that of a liquid.[11] From Fig. 7, it can be observed that in the low-temperature region (T < 483 K), the density of RP-3 is almost the same under different pressures. As the temperature increases, the effect of pressure on the density of RP-3 becomes more pronounced; the higher the pressure, the greater the density of RP-3.

The AAD between the experiment value and the fitted value is 1.09%, 0.80%, and 0.76% at different pressures of 6, 7, and 8 MPa, respectively. The MAD of the RP-3 density fitting results in the supercritical region ($T > 650$ K) at three different pressures is 4.97%, 3.56%, and 2.67%, respectively. These values are all higher than those recorded when the RP-3 temperature is below the pseudo-critical region, which are 1.59%, 1.69%, and 1.34%, respectively. The higher the temperature of RP-3, the greater the deviation in the fitting results. The main factor causing this phenomenon is that closer to the pseudo-critical region, the changes in thermal properties become more dramatic, where minor temperature changes can lead to significant differences in physical properties. This non-uniform distribution of thermal properties might slightly degrade the stability and accuracy of density measurements.

5. Conclusions

This study provides a comprehensive analysis of the density measurement of Chinese aviation kerosene RP-3 with a high-pressure and high-temperature regime. An experimental system for investigating supercritical hydrocarbon fuel flow and heat transfer characteristics has been established. Utilizing an optimized flow method, the density of RP-3 was successfully measured. The measurements covered a pressure range of 6–8 MPa and a temperature range of 323–783 K, marking the first collection of such extensive data under these conditions. The key conclusions are summarized as follows:

(1) The current study has developed a method for measuring fluid density based on the law of mass conservation using a thermal pulse technique, which allows for high-precision measurement of fluid density under high temperature and high pressure conditions. The precision of this measurement technique is validated using n-decane as a calibration fluid, which achieves an average absolute deviation of 0.91%, demonstrating the reliability of the approach.
(2) The density of aviation kerosene RP-3 was experimentally measured for the first time within a pressure range of 6–8 MPa and a temperature range of 323–783 K, with a maximum relative uncertainty of 0.35%. All RP-3 density readings at constant pressures were fitted using a piecewise polynomial. The average absolute deviation between the experiment value and the fitted value of RP-3 density is 1.09%, 0.80%, and 0.76% at different pressures of 6, 7, and 8 MPa, respectively, illustrating the robustness of the fitting approach used.
(3) In the low-temperature region ($T < 483$ K), the density of RP-3 is almost the same under different pressures. As the temperature increases, the effect of pressure on the density of RP-3 becomes more pronounced; the higher the pressure, the greater the density of RP-3.

CRediT authorship contribution statement

Yanchen FU: Writing – review & editing, Methodology, Funding acquisition. **Weitong LIU:** Writing – review & editing, Writing – original draft, Investigation, Formal analysis. **Shenzhou SHI:** Writing – original draft, Software, Data curation. **Ruoyu WANG:** Resources. **Yinlong LIU:** Resources. **Guoqiang XU:** Supervision, Project administration, Conceptualization.

Declaration of competing interest

The authors declare that they have no known competing financial interests or personal relationships that could have appeared to influence the work reported in this paper.

Acknowledgements

This study was supported by the Science Center for Gas Turbine Project, China (No. P2022-C-II-005-001).

References

1. Xu L, Sun ZN, Ruan QC, et al. Development trend of cooling technology for turbine blades at super-high temperature of above 2000 K. *Energies* 2023;**16**(2):668.
2. Risnyk S, Artushenko A, Kravchenko I, et al. Experimental investigation of two competitive high pressure turbine blade cooling systems. New York: ASME; 2017. Report No.: GT2017-64915.
3. Fu YC, Liu WT, Qi H, et al. Heat transfer area optimization of intermediate heat-exchange cycle system for aero engines. *Int J Heat Mass Transf* 2024;**220**:124995.
4. Liu WT, Xu GQ, Fu YC, et al. Numerical investigation on forced, natural, and mixed convective heat transfer of n-decane in laminar flow at supercritical pressures. *Int J Heat Mass Transf* 2023;**209**:124129.
5. van Heerden ASJ, Judt DM, Jafari S, et al. Aircraft thermal management: Practices, technology, system architectures, future challenges, and opportunities. *Prog Aerosp Sci* 2022;**128**:100767.
6. Liu WT, Xu GQ, Gang XJ, et al. Theoretical modeling, experimental validation, and thermodynamic analysis on intermediate heat-exchange cycle system. *Int Commun Heat Mass Transf* 2024;**156**:107635.
7. Bruening GB, Chang WS. Cooled cooling air systems for turbine thermal management.New York: ASME; 1999. Report No.: 99-GT-014.
8. Huang H, Spadaccini L, Sobel D. Fuel-cooled thermal management for advanced aeroengines. *J Eng Gas Turbines Power* 2004;**126**(2):284–93.
9. Fu YC, Liu YL, Wang J, et al. Local resistance characteristics of elbows for supercritical pressure RP-3 flowing in serpentine micro-tubes. *Propuls Power Res* 2024;**13**(2):245–56.
10. Fu YC, Liu WT, Wang J, et al. Experimental investigation on heat transfer enhancement of supercritical pressure aviation kerosene in tubular laminar flow by vibration. *Appl Therm Eng* 2024;**257**:124206.
11. Comstock MJ. *Supercritical fluid engineering science*. Washington, D.C.: ACS Publications; 1992. p. 24–5.
12. Deng HW, Zhu K, Xu GQ, et al. Heat transfer characteristics of RP-3 kerosene at supercritical pressure in a vertical circular tube. *J Enh Heat Transf* 2012;**19**(5):409–21.
13. Sun X, Meng H. Large eddy simulations and analyses of hydrocarbon fuel heat transfer in vertical upward flows at supercritical pressures. *Int J Heat Mass Transf* 2021;**170**:120988.
14. Amiri A, Triplett Z, Moreira A, et al. Standard density measurement method development for flax fiber. *Ind Crops Prod* 2017;**96**:196–202.
15. Koca T. A density measurement device for solid objects with uneven geometry. *Mater Test* 2021;**63**(7):676–80.
16. Decker GE, Bloch ED. Using helium pycnometry to study the apparent densities of metal-organic frameworks. *ACS Appl Mater Interfaces* 2021;**13**(44):51925–32.

17. Elsergany RN, Vreeman G, Sun CC. An approach for predicting the true density of powders based on in-die compression data. *Int J Pharm* 2023;**637**:122875.
18. Zhou ZM, Ren TT, Li M, et al. Study on temperature measurement of petroleum product density analyzer based on hydrometer method. *J Phys: Conf Ser* 2023;**2428**(1):012001.
19. Bakovets NV, Konicheva EN. Measuring liquid density in a system for ensuring uniformity of measurements. *J Belarusian State Univ Phys* 2022;**3**:113–9.
20. Vajjha RS, Das DK, Mahagaonkar BM. Density measurement of different nanofluids and their comparison with theory. *Petrol Sci Technol* 2009;**27**(6):612–24.
21. Bogdan OP, Muraveva OV, Blinova AV, et al. Investigation of density of samples made of thermally expanded graphite by acoustic amplitude-shadow method. *Russ J Nondestruct Test* 2023;**59**(8):857–67.
22. Kilmametov A, Gröger R, Hahn H, et al. Bulk density measurements of small solid objects using laser confocal microscopy. *Adv Mater Technol* 2017;**2**(1):1600115.
23. Tanaka K, Higashi Y, Akasaka R. Measurements of the isobaric specific heat capacity and density for HFO-1234yf in the liquid state. *J Chem Eng Data* 2010;**55**(2):901–3.
24. Bruno T, Huber M, Laesecke A, et al. Thermochemical and thermophysical properties of JP-10. Gaithersburg: National Institute of Standards and Technology; 2006. Report No.: 6640.
25. Chuong HD, Sang TT, Tam HD. Monte Carlo simulation combined with experimental measurements based on gamma transmission technique for determining the density of liquid. *Radiat Phys Chem* 2021;**179**:109216.
26. Lentner R, Eckmann P, Kleinrahm R, et al. Density measurements of seven methane-rich binary mixtures over the temperature range from (100 to 180) K at pressures up to 9.7 MPa. *J Chem Thermodyn* 2020;**142**:106002.
27. Mendo-Sánchez RP, Arroyo-Hernández CA, Pimentel-Rodas A, et al. Simultaneous viscosity and density measurements and modeling of 2-alcohols at temperatures between (291 and 353) K and pressures up to 50 MPa. *Fluid Phase Equilib* 2020;**514**:112559.
28. Concepción EI, Moreau A, Martín MC, et al. Density and viscosity measurements of (piperazine + water) and (piperazine + 2-dimethylaminoethanol + water) at high pressures. *J Chem Thermodyn* 2020;**141**:105960.
29. Safarov J, Lesch F, Suleymanli K, et al. High-temperature and high-pressure density measurements and other derived thermodynamic properties of 1-butyl-3-methylimidazolium tris (pentafluoroethyl) trifluorophosphate. *Thermochim Acta* 2017;**658**:14–23.
30. Santos TVM, Pereira MFV, Avelino HMNT, et al. Viscosity and density measurements on liquid n-tetradecane at moderately high pressures. *Fluid Phase Equilib* 2017;**453**:46–57.
31. Lentner R, Richter M, Kleinrahm R, et al. Density measurements of liquefied natural gas (LNG) over the temperature range from (105 to 135) K at pressures up to 8.9 MPa. *J Chem Thermodyn* 2017;**112**:68–76.
32. Sanmamed YA, González-Salgado D, Troncoso J, et al. Experimental methodology for precise determination of density of RTILs as a function of temperature and pressure using vibrating tube densimeters. *J Chem Thermodyn* 2010;**42**(4):553–63.
33. Aparicio S, Atilhan M, Karadas F. Thermophysical properties of pure ionic liquids: review of present situation. *Ind Eng Chem Res* 2010;**49**(20):9580–95.
34. Krohn NA, Wymer RG. X-ray method for determining liquid densities at high temperatures and pressures. *Anal Chem* 1962;**34**(1):121–3.
35. Sutin AM, Yoon SW, Kim EJ, et al. Nonlinear acoustic method for bubble density measurements in water. *J Acoust Soc Am* 1998;**103**(5):2377–84.
36. Trinh EH, Hsu CJ. Acoustic levitation methods for density measurements. *J Acoust Soc Am* 1986;**80**(6):1757–61.
37. Rechberger A, Amsüss R, Rossegger S, et al. High precision vibration-type densitometers based on pulsed excitation measurements. *Sensors* 2019;**19**(7):1627.
38. Wagner Z, Bendová M, Rotrekl J, et al. Density and sound velocity measurement by an Anton Paar DSA 5000 density meter: precision and long-time stability. *J Mol Liq* 2021;**329**:115547.
39. Gülüm M, Bilgin A. Measurements and empirical correlations in predicting biodiesel-diesel blends' viscosity and density. *Fuel* 2017;**199**:567–77.
40. Wen J, Zhang N, Fu YC, et al. Density measurements of propellant EHF-TU at (3 to 7) MPa supercritical pressures. *J Chem Eng Data* 2018;**63**(6):1961–8.
41. Yang ZQ, Bi QC, Guo Y, et al. Design of a gamma densitometer for hydrocarbon fuel at high temperature and supercritical pressure. *J Chem Eng Data* 2014;**59**(11):3335–43.
42. Deng HW, Zhang CB, Xu GQ, et al. Density measurements of endothermic hydrocarbon fuel at sub- and supercritical conditions. *J Chem Eng Data* 2011;**56**(6):2980–6.
43. Ma HA, Xie MZ, Zeng W, et al. Experimental study on combustion characteristics of Chinese RP-3 kerosene. *Chin J Aeronaut* 2016;**29**(2):375–85.
44. Deng HW, Zhang CB, Xu GQ, et al. Visualization experiments of a specific fuel flow through quartz-glass tubes under both sub- and supercritical conditions. *Chin J Aeronaut* 2012;**25**(3):372–80.
45. Pei XY, Hou LY. Effect of different species on physical properties for the surrogate of aviation fuel. *J Tsinghua Univ* 2017;**57**(7):774–9 [Chinese].
46. Cheng YX, Wang YS, Jiang PX, et al. Oxidative and pyrolytic coking characteristics of supercritical-pressure n-decane and its influence mechanism on heat transfer. *Fuel* 2024;**362**:130874.
47. Zuo Y, Huang HR, Fu YC, et al. Vibration effects on heat transfer characteristics of supercritical pressure hydrocarbon fuel in transition and turbulent states. *Appl Therm Eng* 2023;**219**:119617.
48. Bejan A. *Convection heat transfer*. Hoboken: John Wiley & Sons Inc.; 2013. p. 520–1.
49. Lemmon E, Huber M, McLinden M. *NIST standard reference database 23: Reference fluid thermodynamic and transport properties-REFPROP, version 8.0*. Gaithersburg: National Institute of Standards and Technology; 2007.
50. Wu XH, Moin P. A direct numerical simulation study on the mean velocity characteristics in turbulent pipe flow. *J Fluid Mech* 2008;**608**:81–112.
51. McKeon BJ, Li J, Jiang W, et al. Further observations on the mean velocity distribution in fully developed pipe flow. *J Fluid Mech* 2004;**501**:135–47.